The International Journal of Advanced Manufacturing Technology (2024) 131:5277–5288
https://doi.org/10.1007/s00170-024-13354-9

ORIGINAL ARTICLE

Vacuum-oxygen-low recycling process of aluminium composites manufactured from steel machining chips

Fredrick M. Mwema[1,2] · Job M. Wambua[1] · Michael O. Bodunrin[3] · Tien-Chien Jen[2] · Esther T. Akinlabi[1]

Received: 20 October 2023 / Accepted: 25 February 2024 / Published online: 4 March 2024

Abstract

Metal machining workshops generate a lot of metal chips, which pose both health and disposal challenges. Herein, for the first time, we demonstrate a novel process of reusing lathe-turning steel chips to manufacture high-compression strength Al alloy/steel composites. The process involves melting aluminium alloy onto the steel chips under vacuum and argon gas conditions. Clean and dried steel chips are packed inside a mould with a top layer of aluminium alloy pieces at three different quantity ratios of 80%Al/20% steel, 20%Al/80% steel and 50%Al/50% steel. The steel mould is then heated in a furnace at 650–700 °C until the aluminium metal melts. After a predetermined time of melting, argon gas is bubbled into the top layer (molten aluminium) of the mould while vacuum pumping is activated on the lower side of the mould (steel chips) for 5 min. The sample is allowed to cool within the mould. The composite containing 50%Al/50% steel has the highest mechanical properties with compression strength twice that of the other two samples. The microstructural observations revealed a good bonding between the steel chips and the Al alloy matrix. The study further presents the machinability of the samples, and it is seen that the composites behave like the aluminium matrix alloy during a turning operation and therefore do not require a special machining operation. It is shown that through this method, machining chips of steel can be recycled into high-compression strength metal–metal composites. These materials have the potential for high-compression strength applications such as machine supports and high-impact cushions.

Keywords Aluminium alloy/steel composites · Recycling · Machining · Steel chips · Microstructure

1 Introduction

Metal-cutting industries generate a lot of metallic waste in the form of machining chips. These chips pose both environmental and health risks and as such their disposal and recycling are of critical importance [1]. These metal chips originate from subtractive manufacturing processes such as traditional machining including turning, milling, and shaping. Recycling metal chips is the most attractive method of dealing with the environmental and health risks of such wastes [2]. As such, there are various attempts to convert and reuse metal chips into valuable products. The current state-of-the-art indicates that the focus is on the conversion of metal chips into metal powders for powder metallurgy and related processing. Steel chips have been recycled directly into products through the solid-state sintering process [3]. A study by Mendonca et al. [4] reported on the recycling of stainless-steel chips into metal powders via planetary ball milling; the study presented a full factorial design of the experiment and optimisation of the process and demonstrated that the addition of ceramic materials into the milling process was the most significant parameter of the process. Through planetary milling, Verma et al. [5] demonstrated that scrap steel chips can be processed into nanostructured powders for powder metallurgy applications. An interesting recycling approach of machine chips has been presented by Jordon et al. [6] in which they designed a novel solid-state additive manufacturing to directly convert the chips into additive manufactured products.

✉ Fredrick M. Mwema
fredrick.mwema@northumbria.ac.uk

[1] Department of Mechanical & Construction Engineering, Northumbria University, Newcastle, UK

[2] Department of Mechanical Engineering Science, University of Johannesburg, Johannesburg, South Africa

[3] School of Chemical and Metallurgical Engineering, University of the Witwatersrand, Johannesburg, South Africa

The machine chips have also been recycled to produce composite materials for various applications [7]. A study by Alwaeli and Nadziakiewicz [8] demonstrated the use of steel chips as additives for the manufacturing of concrete products for the construction industry. The study reported that the addition of the chips enhanced the absorption of radiation of the concrete structures. Alaneme and Odoni [9] presented a study on mechanical properties, wear and corrosion behaviour of copper composites reinforced with steel machining chips through stir casting; the influence of the % composition of the steel chips in the copper matrix was investigated. It was demonstrated that an increase in mass % of steel chips enhanced the properties of the copper composite. Vacuum-assisted melt infiltration method has been used to fabricate steel/aluminium composites and interesting properties of the material reported [10]. Of importance in the reuse of chips is the bond strength between the matrix and chips since it determines the overall properties of the composite. It has been reported that oxygen-free and vacuum-based techniques can greatly enhance bond interactions between the matrix and the chips [11] and therefore improve the properties of the composites. In this study therefore, a novel approach which combines both vacuum and oxygen-free conditions is proposed, for the first time, as a technique for recycling of steel machining chips into high-compression strength aluminium-steel composites. An important aspect of the work is that it explored a new approach for recycling of machining steel chips.

2 Materials and methods

In this work, mild steel chips were collected during a turning operation of AISI 1080 steel shafts in a machine workshop. The chips were specifically collected during the machining operation to avoid contamination by other materials and ensure consistency in the presented results. The main composition (% weight) of the AISI 1080 steel shaft as provided by the manufacturer was C (0.30), Mn (0.62%), P (0.02), S (0.01), and Fe (balance). The physical properties of the material are a density of 7.85 g/cm^3, melting point of 1510 °C, yield strength of 440 MPa, and Young's modulus of 210 GPa. The steel chips were then washed in vinegar solution to remove the coolant and oxides after which they were dried in an oven at 80 °C for 3 h. The steel chips were then sieved and graded, and the steel chips used in this work had length sizes of 150 µm and below.

The aluminium alloy-steel (Al/steel) composites were prepared using the apparatus in Fig. 1. The Al–Mg-Si-Cu alloy (Al 6061) (herein referred to as aluminium) was used. The apparatus consists of a tubular chamber fabricated from a steel plate of 5-mm thickness. It has a top inlet connected to the argon gas supply and a lower inlet connected to a vacuum system. In operation, the tubular chamber is usually orientated vertically inside a 700 °C furnace. The dry metal chips were loaded inside the tubular chamber halfway and then filled with small sizes of waste aluminium alloy blocks. The chamber was tightly sealed, and it was then

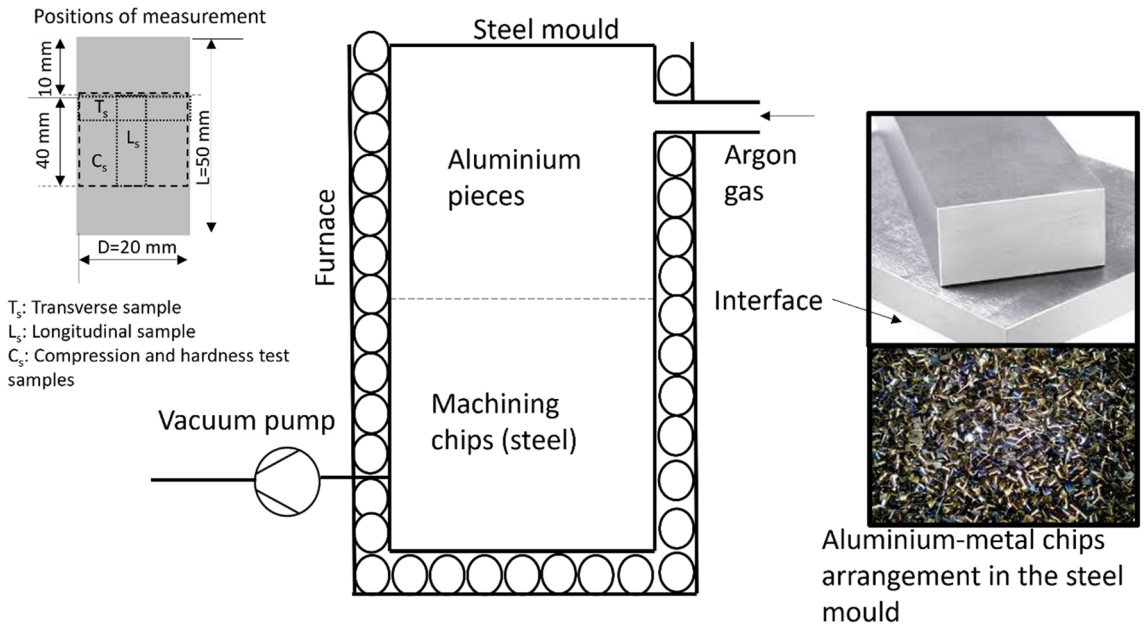

Fig. 1 Illustrating the methodology for the preparation of metal foams from machining chips. The arrangement of the aluminium and chips inside the mould steel is shown. Cylindrical samples of diameter *d* and length *L*, with sampling points for transverse, longitudinal, and compression/hardness samples illustrated

placed inside the furnace as shown in Fig. 1. The chamber and its content were exposed to temperatures between 600 and 700 °C until all the aluminium blocks melted. Then, the argon gas and vacuum pumps were activated while maintaining the heating for about 20 min. The vacuum pump and furnace were simultaneously switched off, and the tubular chamber was allowed to cool under argon gas for 5–8 min after which the argon gas pump was switched off and the material was then removed from the chamber and allowed to cool in air. This was followed by cutting off the protruding layer of the metal chips on the lower side of the circular sample (shown in Fig. 1). The obtained samples (shown as insert in Fig. 1) were 20-mm diameter and 60-mm length. The samples for microstructural and mechanical measurements were obtained at a longitudinal location of 10 mm from the top of the fabricated samples (as shown in Fig. 1). The samples were prepared at different weight proportions: 20 wt.% steel/80 wt.% Al, 50 wt.% steel/50 wt.% Al, and 80 wt.% Al/20 wt.% steel.

The samples were ground on the surfaces using SiC paper starting from a grit size of #200 to #2000. The samples were then polished using diamond pastes of 15 µm, 6 µm, 3 µm, and finally by 1 µm grain sizes. The samples were then polished to a mirror finish using a colloidal oxide suspension of ¼ µm grain size. The microstructures of the samples were then obtained using optical and scanning electron (SEM) microscopes. The mechanical properties were measured using Rockwell hardness and compression tests on a universal tensile machine (INSTRON 3365, INSTRON) and according to the respective ASTM standards. For each hardness, ten points readings on different points of the sample were taken whereas for tensile and compression test six samples were analysed for statistical accuracy. The machinability of the composites was evaluated by the design of experiment (DOE) for a turning operation consisting of two factors (spindle speed and depth of cut) and three levels of each factor, i.e. spindle speed (460 rpm, 755 rpm, and 1255 rpm) and depth of cut (0.4 mm, 0.7 mm, and 1.0 mm). An L9 orthogonal array was produced from the design, which produced nine experimental combinations. The machining was evaluated for material removal rate (MRR), chip type, and surface roughness.

3 Results and discussion

3.1 Mechanical characterisation

The mechanical properties of the prepared samples were characterised via hardness and compression tests (ASTM E209-18). The microhardness in terms of Rockwell microhardness (HRC) number and compression tests for the samples prepared with 20 wt.% steel/80 wt.% Al, 50 wt.% steel/50 wt.% Al, and 80 wt.% steel/20 wt.% Al are presented in Table 1. The hardness values shown were taken on the transverse (diameter surface). The hardness values along the length (longitudinal) were very random and very low (~ 20 HRC) due to non-homogeneity in microstructure as it will be seen in the next section of the paper. Sample consisting of 50 wt.% Al/50 wt.% steel of constituents exhibited the highest hardness and compression strength; hence, it was therefore investigated further for microstructure in the next section. The high mechanical properties of this sample can be attributed to the synergistic effects from both aluminium and steel. The combination of aluminium's high strength-to-weight ratio and steel's toughness can result in an alloy with improved overall mechanical properties; since Al is ductile and steel is tough (and brittle), a 50% composition indicates a good balance of these properties. Additionally, in the 50% Al-50% steel composite, there is a balanced mixture of aluminium and steel. This balance can lead to a more homogeneous microstructure (as it will be seen in microstructure analyses), potentially resulting in solid solution strengthening. As such, there is a good balance between ductility and toughness. A very high concentration of steel (80%) leads to formation of a brittle structure and hence very low deformation behaviour. A sample with very low concentration of steel (20% steel-80% Al) exhibits a higher ductility and very low toughness and hence lower mechanical strength than 50% steel-50% Al composites and higher strength than 80% steel-20% Al composites.

3.2 Microstructure characterisation for 50 wt.% aluminium-50 wt.% steel samples

The microstructure of the developed steel chips/aluminium composites was observed using both optical and scanning electron microscopes. The micrographs were taken on surfaces along the length (L) and diameter (d) of the samples. The optical micrographs (Fig. 2) show the differences in morphology and distribution of the microstructural features along the length and diametral directions. Along the length of the samples, in Fig. 2a, elongated (white) eutectic phase which is denoted as ***A*** is randomly distributed on the surface of the composite. This eutectic phase also appears as a nearly circular morphology which

Table 1 Rockwell hardness and compression strength properties of the aluminium/steel chip composites

Sample	Hardness (HRC)	Compression strength (MPa)
20 wt.% steel/80 wt.% Al	48.68 ± 6.52	50 ± 0.32
50 wt.% steel/50 wt.% Al	52.84 ± 2.98	90 ± 0.15
80 wt.% steel/20 wt.% Al	41.62 ± 1.14	48 ± 0.10

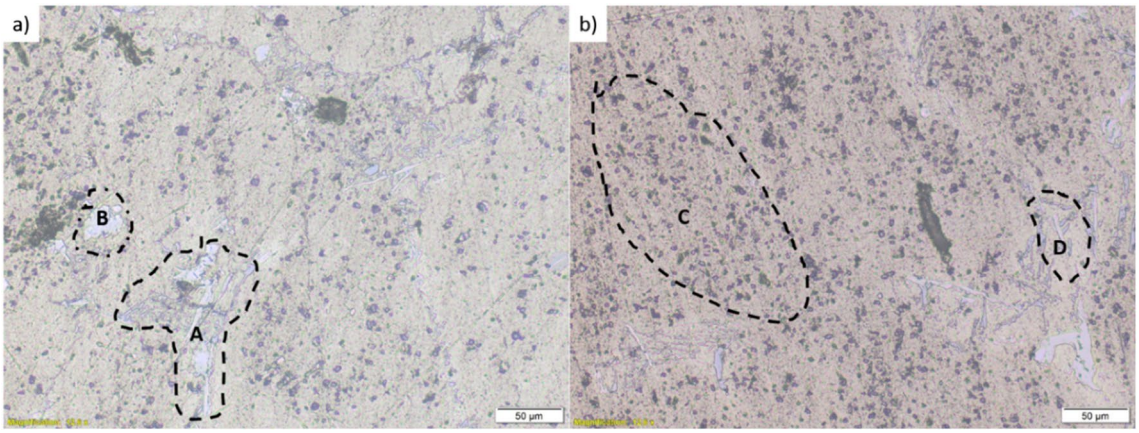

Fig. 2 Optical micrographs of the 50 wt.% aluminium/50 wt.% steel chip composites taken on surfaces along the **a** length (*L*) and **b** diameter (*d*) of the cylindrical samples

can also be (denoted as ***B***) observed along the length of these samples. These morphologies can be attributed to the thermal, pressure, and concentration gradients during solidification of the molten aluminium around the steel chips. Some of the molten aluminium got trapped between the chains of the steel chips cooling rapidly to form eutectic phase of blocky and elongated morphologies. The micrographs taken on the surfaces along the diameter (*d*) of the samples, Fig. 2b, show a uniformly distributed particle-like dark intermetallic phase, denoted as ***C*** although a few agglomerated and elongated particles (shown as ***D***) can also be observed.

The SEM images of the two surfaces are shown in Fig. 3, and the microstructure generally captured three phases, *i.e.* the steel reinforcement, aluminium matrix, and the interface. Figure 3a shows the microstructure taken along the length of the samples where the iron-rich region is denoted as B and H, whereas the aluminium-rich region is denoted as A. The B region is slightly darker than H which indicates there might be slight variations in chemical composition, thus making H a possible interfacial region. The particles within the structure appear non-uniform in terms of distribution and morphology. As for the SEM image taken at across the diameter of the sample (Fig. 3b), the particles denoted as **C** are well-dispersed within the matrix and iron-rich phase with irregular morphology denoted as **D** is observed.

Figures 4 and 5 indicate phases where compositional analyses were done along the length and diameter respectively. The respective compositions are presented in Tables 1 and 2, respectively. In Table 1, the composition of the phases along the length of the sample is presented. It is observed that the light phase is the iron-rich region, denoted as 1. At grain boundary of the iron-rich phase is

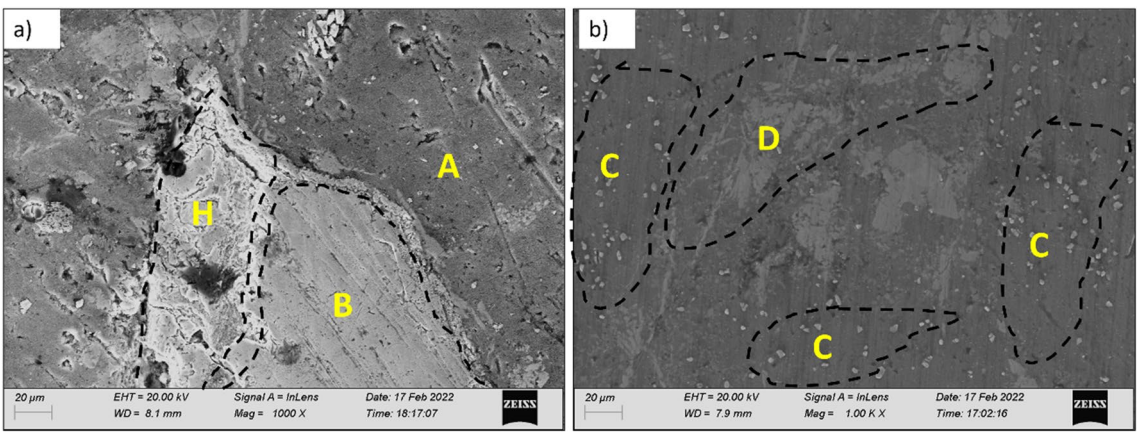

Fig. 3 SEM micrographs of the 50 wt.% aluminium/50 wt.% steel chip composites taken on surfaces along the **a** length and **b** diameter of the cylindrical samples

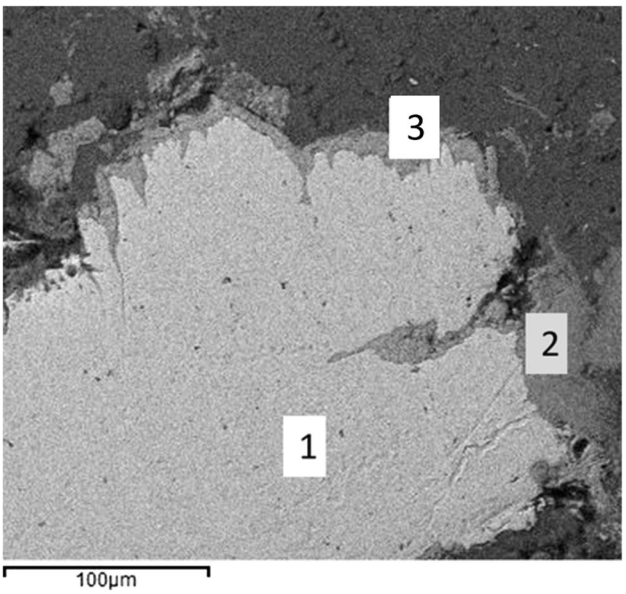

Fig. 4 SEM image showing the EDS chemical composition measurements at points 1, 2, and 3 along the length of the 50 wt.% steel chips/50 wt.% aluminium

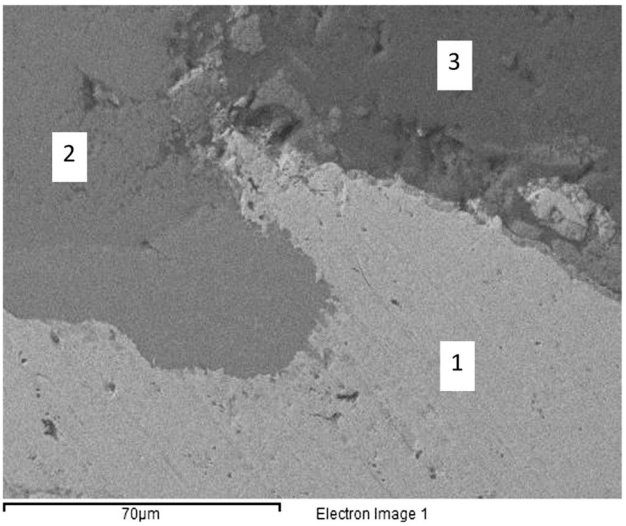

Fig. 5 SEM image of the surface of diameter of 50 wt.% steel chips/50 wt.% aluminium composites showing the regions on which EDS was undertaken

an interfacial region denoted as region 2; the ratio of Fe to Al based on compositional analysis is approximately 1:2.6. Small amount of silicon and manganese is present at this interface. Next to the interfacial region is an aluminium-rich phase with small amount of silicon copper and oxygen. Table 2 presents the composition of the similar phases that were identified previously, albeit this represents the composition taken along the diameter of the sample. Again, the light phase (region 1) is rich in iron, indicating

Table 2 EDS chemical composition of the composites along the length surfaces (50 wt.% steel chips/50 wt.% aluminium)

Elements	Chemical composition (atomic (%))		
	Region 1	Region 2	Region 3
Al K	1.95	70.62	91.07
Si K	–	1.77	1.26
Mn K	0.39	0.28	–
Fe K	97.66	27.32	–
Cu K	–	–	0.59
O K	–	–	7.09
Totals	100	100	100

Table 3 EDS chemical composition of the composites on the diametral surface (50 wt.% steel chips/50 wt.% aluminium)

Elements	Chemical composition (atomic (%))		
	Region 1	Region 2	Region 3
Al K	1.22	69.13	97.94
Si K	0.47	12.43	1.60
Mn K	0.45	–	–
Fe K	97.87	18.43	–
Cu K	–	–	0.46
Totals	100	100	100

the reinforcing phase, the interfacial region (region 2) has Fe:Al ratio of 1:3.8, while the dark phase is aluminium rich containing small amount of silicon and copper. This dark phase is the matrix of the composites. The variation in the ratio iron to aluminium in the interfacial region indicates that there exists diffusion gradient relative to the diameter and length of the sample. This may have significant implication on the bonding of Al matrix to the steel chip reinforcement. It appears that the higher Fe:Al ratio at the interface offers superior interfacial bonding in the lateral section for the composites since more molten aluminium would be available to wet the steel chip. The integrity of the interfacial bonding between the matrix and the reinforcing material is considered in the next section.

Similarly, Fig. 5 and Table 3 show the composition of the various phases on the diametral surfaces of the 50 wt.% steel chips/50 wt.% aluminium composite. It can be observed that in these surfaces the composite consists of similar phases as the length of the composites, i.e. Fe-dominant phases (*denoted as* 1 in Fig. 5), Al-dominant phases (*denoted as* 3 in Fig. 5), and Al–Fe (*denoted as* 2 in Fig. 5). The only difference between results in Tables 1 and 2 is that there were more (constituent) chemical elements obtained on the diametral surfaces (Table 3) than along the length. This is an indication of incomplete flow of molten aluminium during fabrication of the samples.

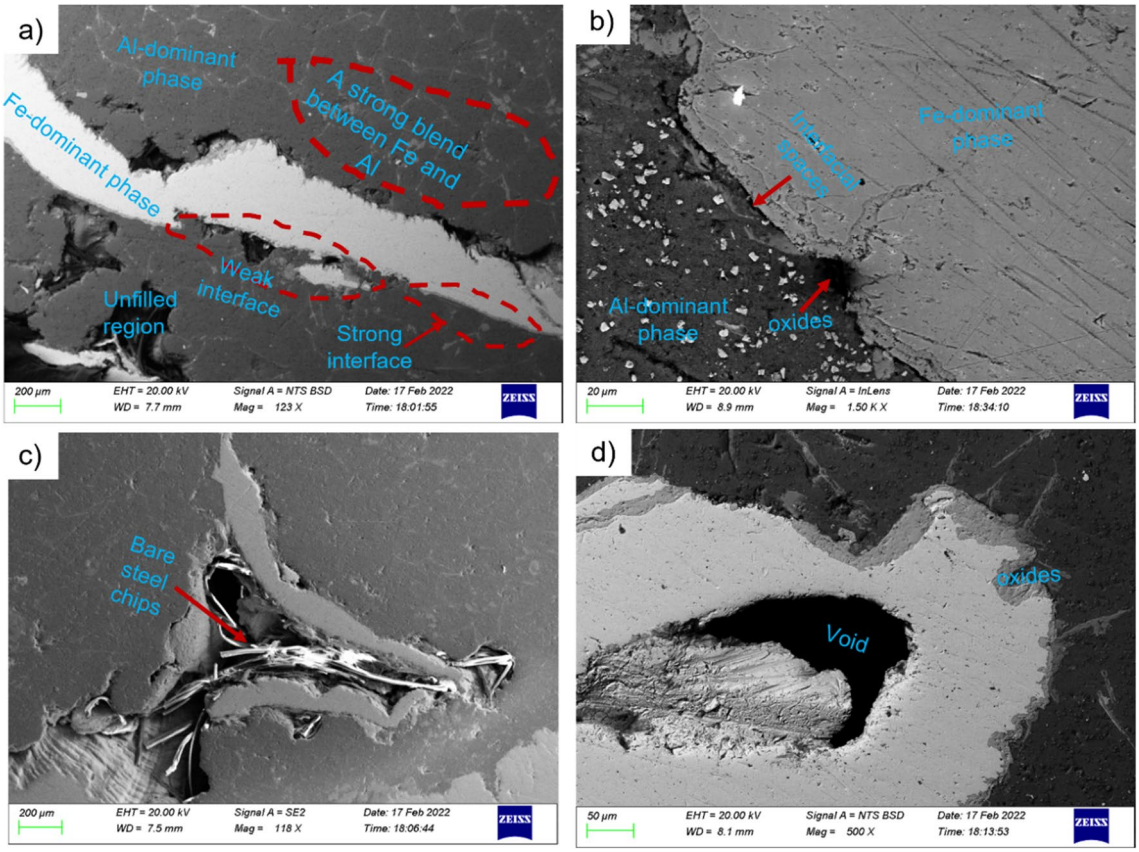

Fig. 6 Detailed SEM microstructural observations along the length (L) of the 50 wt.% steel chips/50 wt.% aluminium samples. **a** A backscatter image showing the interfacial voids and unfilled regions. **b** A secondary image (at higher magnification) showing oxides at the interfaces. **c** A low-magnification secondary image showing surfaces of steel chips without aluminium phases. **d** A backscatter image showing voids and oxides within the unfilled regions of the samples. The images were taken at different magnifications to detail various structures along the length of the composites

Figure 6 shows a detailed analysis of the cross section of the samples along the length (L). It should be noted that the images have been taken at different magnifications along the length of the samples for purposes of detailing structural interactions among the phases as identified in Fig. 4. As shown, the structure consists of various structures within the two-phase dominated microstructure. Between the steel-dominant (Fe) phase and Al-dominant phase, there are both weak and strong interfacial bonds (as shown by the backscattered image in Fig. 6a). At higher magnification, it is observed that these weak bonds consist of discontinuous voids, spaces, and oxides (as shown by secondary image in Fig. 6b). At a very low magnification of secondary imaging, morphologies of bare steel chip surfaces (Fig. 6c) can be observed intertwined within unfilled spaces and voids, which have been identified via a backscattered image in Fig. 6d. These results demonstrate that the molten aluminium did not flow fully (by gravity and difference in pressure) through the length of the mould to blend/bond with steel chips. As such, the microstructure is characterised by heterogeneity in terms of the distribution and morphology of the structures along the length of the samples. However, along the diameter surfaces, the microstructure appears more uniform with few deformities as highlighted by red dotted shapes in Fig. 7a and spongy-like structures (shown as E in Fig. 7b) at the interface between steel chips and aluminium phases. This implies that the flow, and hence coverage, of molten aluminium along the diameter was better than along the length of the mould during the production of the samples. These observations demonstrate significant differences in microstructure formation in the transverse and lateral directions of the mould, and therefore, it should be an important consideration during the process.

3.3 Machining evaluation of the composites

The turning operation was undertaken on a typical lathe machine for the samples consisting of the three compositions and results are presented in Tables 4, 5, and 6. As shown, the

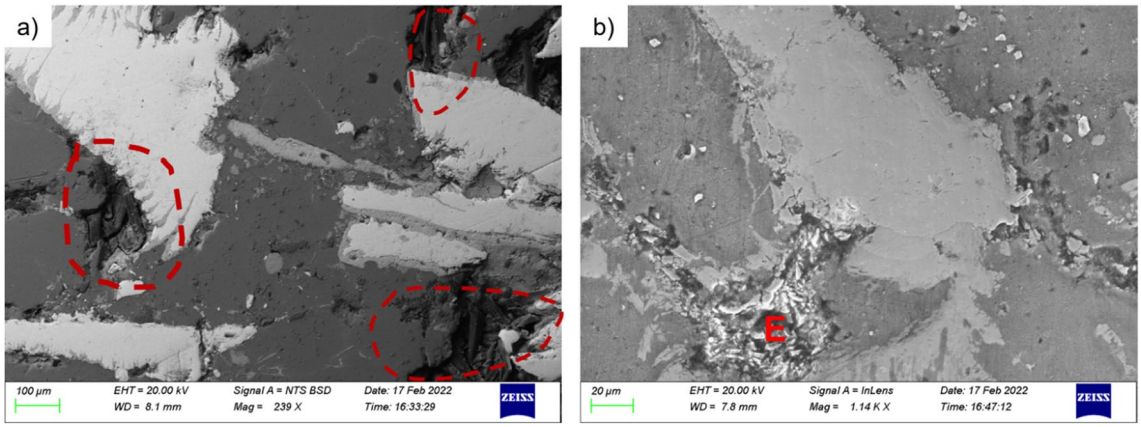

Fig. 7 Detailed SEM microstructural observations along the diameter (*D*) of the 50 wt.% steel chips/50 wt.% aluminium samples. The microstructure appears less heterogenous. **a** Backscatter image (at low magnification) showing deformities of early-solidified aluminium material (marked by red marks) and **b** a high magnification secondary image showing spongy-like phases of steel chips (shown as E). The images have been taken at different magnifications for purposes of detailing the observations on the diameter of the samples

Table 4 Machining results for 80 wt.% Al/20 wt.% steel chips

Experiment	Spindle speed (rpm)	Depth of cut (mm)	Chip type	MRR (g/s)	Average Ra (µm)
1	460	0.4	Discontinuous	0.205	4.383
2	460	0.7	Discontinuous	0.171	5.265
3	460	1.0	Discontinuous	0.114	5.462
4	755	0.4	Continuous with built-up edges	0.160	3.426
5	755	0.7	Continuous with built-up edges	0.158	3.567
6	755	1.0	Continuous with built-up edges	0.098	3.725
7	1255	0.4	Continuous	0.113	3.978
8	1255	0.7	Continuous	0.231	4.113
9	1255	1.0	Continuous	0.469	4.269

Table 5 Machining results for 20 wt.% Al/80 wt.% steel chips

Experiment	Spindle speed (rpm)	Depth of cut (mm)	Chip type	MRR (g/s)	Average Ra (µm)
1	460	0.4	Discontinuous	0.090	3.428
2	460	0.7	Discontinuous	0.099	3.499
3	460	1.0	Discontinuous	0.196	3.511
4	755	0.4	Continuous with built-up edges	0.047	3.189
5	755	0.7	Continuous with built-up edges	0.052	3.267
6	755	1.0	Continuous with built-up edges	0.333	3.300
7	1255	0.4	Continuous	0.097	2.963
8	1255	0.7	Continuous	0.191	3.000
9	1255	1.0	Continuous	0.774	3.020

chip type, material removal rate and average surface roughness were presented as the response outputs for the turning operation. From the tables, the continuous chips were obtained at the highest spindle speed for all values of the depth of cut. This observation corroborates most machining operations for metallic alloys [12]. The result is an indication that the composite can be effectively machined at higher speed speeds.

Table 6 Machining results for 50 wt.% Al/50 wt.% steel chips

Experiment	Spindle speed (rpm)	Depth of cut (mm)	Chip type	MRR (g/s)	Average Ra (μm)
1	460	0.4	Discontinuous	0.074	3.618
2	460	0.7	Discontinuous	0.099	3.697
3	460	1.0	Discontinuous	0.183	3.725
4	755	0.4	Continuous with built-up edges	0.161	3.269
5	755	0.7	Continuous with built-up edges	0.186	3.299
6	755	1.0	Continuous with built-up edges	0.297	3.315
7	1255	0.4	Continuous	0.219	3.097
8	1255	0.7	Continuous	0.379	3.121
9	1255	1.0	Continuous	0.608	3.183

4 The Taguchi analysis

The analysis of the machining results for the material removal rate (MRR) and the average surface roughness (Ra) was conducted using the Taguchi analysis in Minitab 19 software. The signal-to-noise ratios (SN) were adopted in the analysis. To generate the SN for the MRR, the larger-is-better criterion was selected since the goal was to maximise the material removal rate. On the other hand, the smaller-is-better criterion was selected for the generation of SN of the surface roughness (Ra) since the surface with the lowest value of surface roughness was desired. These two criteria are presented in Eqs. (1) and (2), respectively.

$$\mathrm{SN(for\ MRR)} = -10\log[\frac{1}{n}\sum_{i=0}^{n}\frac{1}{yi^2} \quad (1)$$

$$\mathrm{SN\ (for\ Ra)} = -10\log[\frac{1}{n}\sum_{i=0}^{n}yi^2 \quad (2)$$

The signal-to-noise ratios for the three composites are displayed in Tables 7, 8, and 9.

A response table for the SN for the three composites was also generated to visualise the best machining parameters for each response output. The ranking of the effects of each machining parameter is also presented following the delta values (Table 10).

The largest values of SN ratios for each machining parameter for the three composites are bolded in Table 10. These ratios represent the optimal machining parameters for each composite [13]. These optimal machining parameters are summarised in Table 11. The main effect plots for the material removal rates and surface roughness of the three composites are also shown in Figs. 8 and 9, respectively. The plots display the impacts of the machining parameters on the specific responses and the optimal levels of these machining parameters.

The machinability behaviour of the three composites is similar as displayed by the optimal parameters in Table 11. For the optimal material removal rate, the optimal parameters, as expected, are the highest since the quantity of the material removed is a factor of the machining parameters [13]. An increase in spindle speed and depth of cut increases the tool-workpiece contact area and hence the

Table 7 SN ratios for 80 wt.% Al/20 wt.% steel

Experiment	Spindle speed (rpm)	Depth of cut (mm)	MRR (g/s)	Average Ra (μm)	S/NRs for MRR	S/NRs for Ra
1	460	0.4	0.205	4.383	− 13.765	− 12.835
2	460	0.7	0.171	5.265	− 15.340	− 14.428
3	460	1.0	0.114	5.462	− 18.862	− 14.747
4	755	0.4	0.160	3.426	− 15.918	− 10.696
5	755	0.7	0.158	3.567	− 16.027	− 11.046
6	755	1.0	0.098	3.725	− 20.176	− 11.423
7	1255	0.4	0.113	3.978	− 18.938	− 11.993
8	1255	0.7	0.231	4.113	− 12.728	− 12.283
9	1255	1.0	0.469	4.269	− 6.577	− 12.607

Table 8 SN ratios for 20 wt.% Al/80 wt.% steel chips

Experiment	Spindle speed (rpm)	Depth of cut (mm)	MRR (g/s)	Average Ra (μm)	S/NRs for MRR	S/NRs for Ra
1	460	0.4	0.090	3.428	− 20.915	− 10.701
2	460	0.7	0.099	3.499	− 20.087	− 10.879
3	460	1.0	0.196	3.511	− 14.155	− 10.909
4	755	0.4	0.047	3.189	− 26.558	− 10.073
5	755	0.7	0.052	3.267	− 25.680	− 10.283
6	755	1.0	0.333	3.300	− 9.551	− 10.370
7	1255	0.4	0.097	2.963	− 20.265	− 9.435
8	1255	0.7	0.191	3.000	− 14.379	− 9.542
9	1255	1.0	0.774	3.020	− 2.225	− 9.600

Table 9 SN ratios for 50 wt.% Al/50 wt.% steel chips

Experiment	Spindle speed (rpm)	Depth of cut (mm)	MRR (g/s)	Average Ra (μm)	S/NRs for MRR	S/NRs for Ra
1	460	0.4	0.074	3.618	− 22.615	− 11.169
2	460	0.7	0.099	3.697	− 20.087	− 11.357
3	460	1.0	0.183	3.725	− 14.751	− 11.423
4	755	0.4	0.161	3.269	− 15.864	− 10.288
5	755	0.7	0.186	3.299	− 14.610	− 10.368
6	755	1.0	0.297	3.315	− 10.545	− 10.410
7	1255	0.4	0.219	3.097	− 13.191	− 9.819
8	1255	0.7	0.379	3.121	− 8.427	− 9.886
9	1255	1.0	0.608	3.183	− 4.322	− 10.057

Table 10 Response table of the SN ratios of the MRR and Ra for the three machined composites

Level	80 wt.% Al/20 wt.% steel chips		20 wt.% Al/80 wt.% steel chips		50 wt.% Al/50 wt.% steel chips	
	Spindle speed	Depth of cut	Spindle speed	Depth of cut	Spindle speed	Depth of cut
Material removal rate						
1	− 15.99	− 16.21	− 18.386	− 22.579	− 19.151	− 17.223
2	− 17.37	**− 14.70**	− 20.596	− 20.049	− 13.673	− 14.375
3	**− 12.75**	− 15.20	**− 12.290**	**− 8.644**	**− 8.647**	**− 9.873**
Delta	4.63	1.51	8.307	13.936	10.504	7.351
Rank	1	2	2	1	1	2
Surface roughness						
1	− 14.00	**− 11.84**	− 10.829	**− 10.070**	− 11.316	**− 10.425**
2	**− 11.05**	− 12.59	− 10.242	− 10.235	− 10.355	− 10.537
3	− 12.29	− 12.93	**− 9.526**	− 10.293	**− 9.920**	− 10.630
Delta	2.95	1.08	1.304	0.223	1.396	0.204
Rank	1	2	1	2	1	2

material removal rate. Similarly, the surface roughness of the machined samples is consistent with machining expectations. The optimal machining parameters of the three composites are obtained from high spindle speeds and low depths of cut. An increase in the spindle speed increases the rate of material removal, as earlier discussed, which allows for quicker chip removal [8]. This facilitates quicker heat removal from the machining interface and less damage of the

Table 11 Summary of the optimal machining parameters

Parameter	Material removal rate			Surface roughness		
	80 wt.% Al/20 wt.% steel chips	20 wt.% Al/80 wt.% steel chips	50 wt.% Al/50 wt.% steel chips	80 wt.% Al/20 wt.% steel chips	20 wt.% Al/80 wt.% steel chips	50 wt.% Al/50 wt.% steel chips
Spindle speed (rpm)	1255	1255	1255	755	1255	1255
Depth of cut (mm)	0.7	1.0	1.0	0.4	0.4	0.4

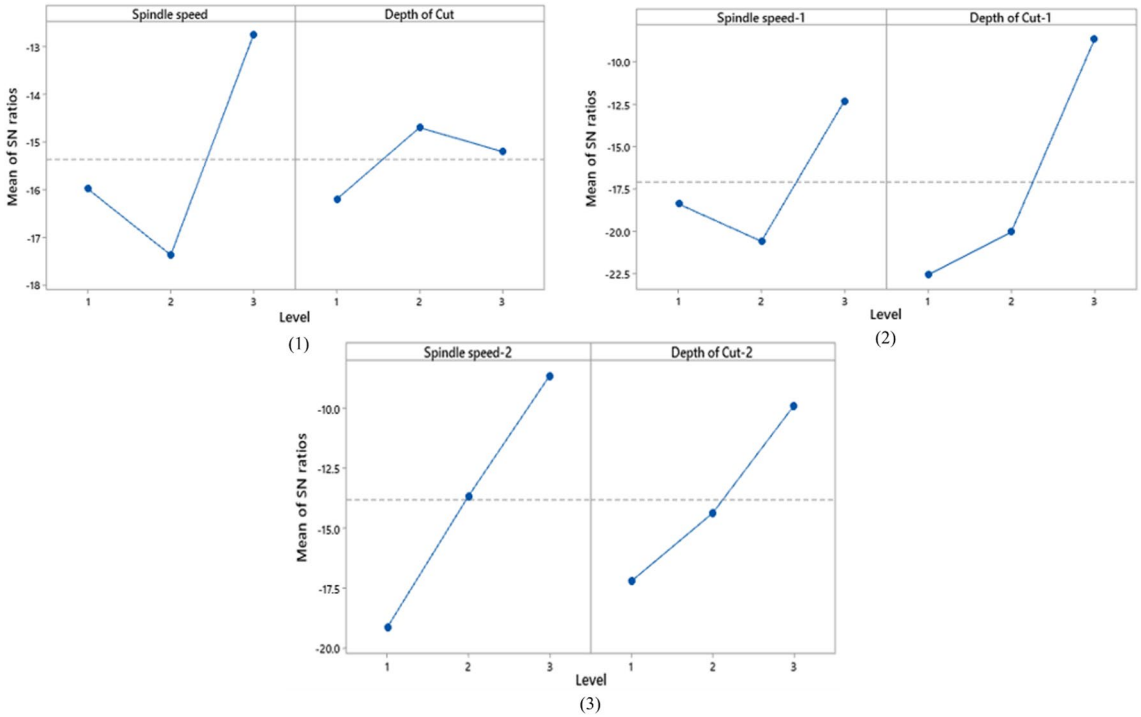

Fig. 8 Main effect plots for SN ratios of MRR for the three composites (larger-is-better) (1) 80 wt.% Al/20 wt.% steel chips, (2) 20 wt.% Al/80 wt.% steel chips, and (3) 50 wt.% Al/50 wt.% steel chips

machined surfaces leading to a better surface finish. Moreover, lower depths of cut are attributed to lower machining forces due to the lower contact area between the cutting tool and the workpiece. These lower forces result in lower machining vibrations and hence a better surface finish, especially for aluminium alloys [14].

The plots in Figs. 8 and 9 show a direct relationship between the spindle speed, material removal rate, and surface roughness for all the three composites. For instance, the main effect plots for the MRR for 80% Al/20% steel chip composite and 20% Al/80% steel chip composite show increasing values of SN ratios as the spindle speed increases. These values trend towards the optimal one, which shows that higher speeds contribute largely to more removal of the material during machining. This could be attributed to increased tool-workpiece contact and increased flow of chips. Moreover, increased speeds seem to produce lower roughness of the machined surfaces, which could be linked to, as earlier stated, a smooth flow of chips which aids in heat dissipation [15].

Consequently, the depth of cut seems to affect the material removal rate positively. From Fig. 8, an increase in the depth of cut increases the SN ratios and hence an increase in the MRR. High depths of cut translate into high surface contacts between the cutting tools and the workpiece surfaces. This trend is more vivid for composites 20% Al/80 steel chips and 50% Al/50% steel chips. The relationship between the depth of cut and the MRR seems to be affected by the high aluminium content in the 80% Al/20% steel chip sample. This is observed from the change in trend once the depth of cut exceeds 0.7 mm (Fig. 8). This could be attributed to

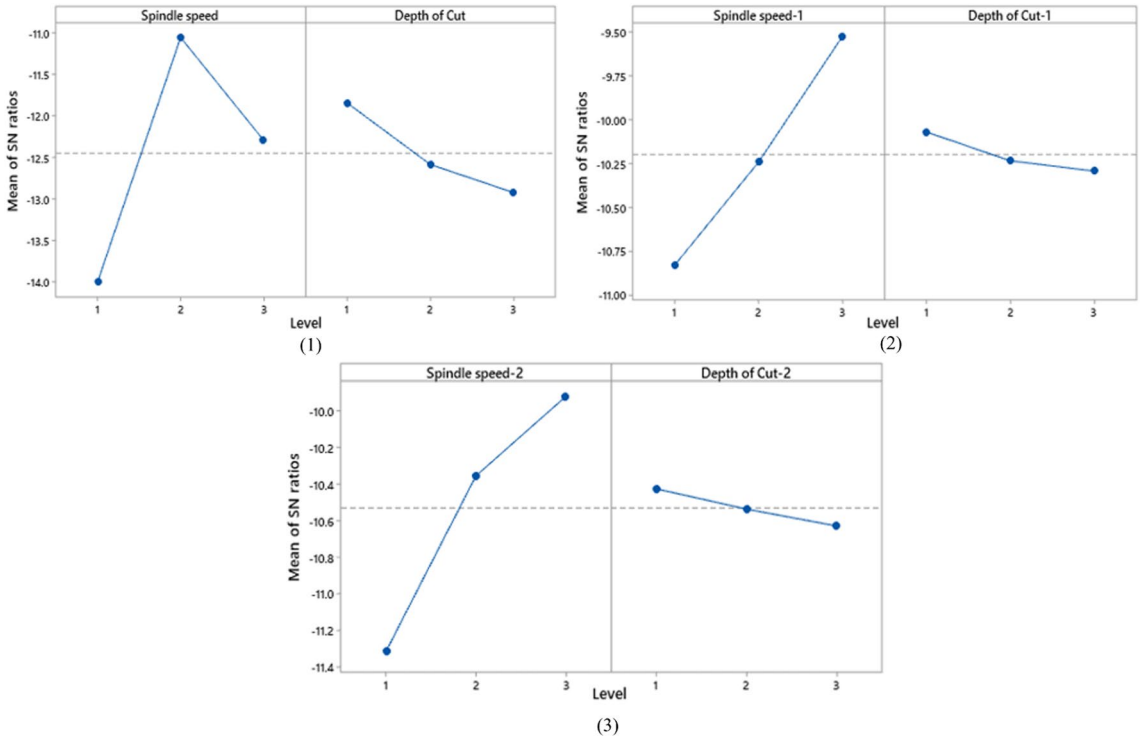

Fig. 9 Main effect plots for SN ratios of Ra for the three composites (smaller-is-better) (1) 80 wt.% Al/20 wt.% steel chips, (2) 20 wt.% Al/80 wt.% steel chips, and (3) 50 wt.% Al/50 wt.% steel chips

the increased cutting area, which limit heat removal creating built-up edges (BUEs) [15].

The 20% Al/80% steel chip composite exhibits the highest MRR of approximately 0.774 g/s, followed by the 50% Al/50% steel (0.608 g/s) and, lastly, composite 80% Al/20 steel (0.469 g/s). This displays that the volume of aluminium in the composite significantly affects its machinability. This could be attributed to the soft nature of aluminium, which create BUEs on the tool and hence limiting removal of materials. On the other hand, the high MRR could have occurred due to the 'crushing effect' of the steel chips in the matrix resulting from the effect of the cutting force. The higher the % of steel, the higher the MRR during machining. The best surface finish was obtained from 20% Al/80% steel (Experiment 7, 2.963 µm). This composite experienced the least surface roughness, which was obtained using the highest spindle speeds and lowest depths of cuts.

In terms of chip formation, the spindle speed seemed to be the most significant determinant for all the three composites. An increase in spindle speed from 460 to 1255 rpm changed the type of chips formed from discontinuous to continuous. This led to increased values of MRR and reduced surface roughness, as the chips could easily flow from the tool-workpiece interface.

5 Conclusions

In this paper, a method of recycling machining steel chips has been presented. The method involves melting aluminium and steel chips within vacuum and argon gas conditions. The obtained samples were characterised for mechanical, microstructure and machinability. The samples containing 50% Al/50% steel by weight were shown to exhibit the attractive mechanical strength. The microscopy observations revealed presence of Fe-dominant, interfacial, and Al alloy-dominant phases, indicating bond formation between Al alloy and steel chips. The composite was further evaluated for machinability on a lathe turning operation. It is demonstrated that the highest cutting speed resulted into better surface finish and continuous chip formation, which means that the developed composite can be machined via the traditional processes and does not require special machining operations. The presented method can be adopted by machining industries to recycle steel chips for components' fabrication, especially those finding applications in high-compression strength applications. Further work shall focus on improving the homogeneity along the longitudinal direction of the samples.

Acknowledgements The authors are grateful to Mr. Kennedy Kipkirui; Mr. Vincent Kiplangat; and Mr. Nahashon Ng'ang'a for their support during the fabrication of the recycling system.

Author contribution Fredrick M Mwema: conceptualisation, experiments, analyses, article writing and submission.
Job Wambua: conceptualisation, analyses, article writing.
Michael Bodunrin: characterisations, article review.
Tien-Chien Jen: article review, supervision.
Esther Akinlabi: article review, supervision.

Funding There was no funding provided for this research.

Declarations

Competing interests The authors declare no competing interests.

References

1. Dhiman S et al (2021) A framework for effective and clean conversion of machining waste into metal powder feedstock for additive manufacturing. Clean Eng Technol 4:100151. https://doi.org/10.1016/j.clet.2021.100151
2. Haider J, Hashmi MSJ (2014) 8.02 - health and environmental impacts in metal machining processes. In: Hashmi S, Batalha GF, Van Tyne CJ, Yilbas B (eds) In: Comprehensive Materials Processing. Elsevier, Oxford, pp 7–33
3. Yao B, Zhou Z, Duan L, and Xiao Z (2016) Compressibility of 304 stainless steel powder metallurgy materials reinforced with 304 short stainless steel fibers. Materials 9(3). https://doi.org/10.3390/ma9030161
4. Mendonça C et al (2019) Recycling chips of stainless steel using a full factorial design. Metals 9(8): 842. [Online]. Available: https://www.mdpi.com/2075-4701/9/8/842. Accessed 15 Sept 2023
5. Verma P, Saha R, Chaira D (2018) Waste steel scrap to nanostructured powder and superior compact through powder metallurgy: powder generation, processing and characterization. Powder Technol 326:159–167. https://doi.org/10.1016/j.powtec.2017.11.061
6. Jordon JB et al (2020) Direct recycling of machine chips through a novel solid-state additive manufacturing process. Mater Design 193:108850. https://doi.org/10.1016/j.matdes.2020.108850
7. Rai A, Prabakar J, Raju CB, Morchalle RK (2002) Metallurgical slag as a component in blended cement. Construct Build Mater 16(8):489–494. https://doi.org/10.1016/S0950-0618(02)00046-6
8. Alwaeli M, Nadziakiewicz J (2012) Recycling of scale and steel chips waste as a partial replacement of sand in concrete. Construct Build Mater 28(1):157–163. https://doi.org/10.1016/j.conbuildmat.2011.08.047
9. Alaneme KK, Odoni BU (2016) Mechanical properties, wear and corrosion behavior of copper matrix composites reinforced with steel machining chips. Eng Sci Technol Int J 19(3):1593–1599. https://doi.org/10.1016/j.jestch.2016.04.006
10. Gecu R, Karaaslan R (2020) Casting temperature dependent wear and corrosion behavior of 304 stainless steel reinforced A356 aluminium matrix bimetal composites fabricated by vacuum-assisted melt infiltration casting. Wear 446–447:203183. https://doi.org/10.1016/j.wear.2020.203183
11. Batista CD, Fernandes A, Vieira MTF, and Emadinia O (2021) From machining chips to raw material for powder metallurgy-a review. Materials (Basel) 14(18). https://doi.org/10.3390/ma14185432
12. Li A, Zhao J, Hou G (2017) Effect of cutting speed on chip formation and wear mechanisms of coated carbide tools when ultra-high-speed face milling titanium alloy Ti-6Al-4V. Adv Mech Eng 9(7):1687814017713704. https://doi.org/10.1177/1687814017713704
13. Surya MS (2022) Optimization of turning parameters while turning Ti-6Al-4V titanium alloy for surface roughness and material removal rate using response surface methodology. Mater Today: Proc 62:3479–3484. https://doi.org/10.1016/j.matpr.2022.04.300
14. Asha PB, Rao CRP, Kiran R, Kumar DVR (2018) Effect of machining parameters on cutting tool temperature and tool life while turning EN24 and Hchcr grade alloy steel. Mater Today: Proc 5(5 Part 2):11819–11826. https://doi.org/10.1016/j.matpr.2018.02.152
15. Kumar S, Saravanan I, Patnaik L (2020) Optimization of surface roughness and material removal rate in milling of AISI 1005 carbon steel using Taguchi approach. Mater Today: Proc 22:654–658. https://doi.org/10.1016/j.matpr.2019.09.039